Innovative sequential combination of fixed bed adsorption/desorption and photocatalysis cost-effective process to remove antibiotics in solution

Sarra Karoui[a,b,c], Rim Ben Arfi[a], Achraf Ghorbal[a,d], Abdeltif Amrane[c], Aymen Amine Assadi[c,*]

[a] Research Laboratory LR18ES33, National Engineering School of Gabes, University of Gabes, Tunisia

[b] National Engineering School of Sfax, University of Sfax, Tunisia

[c] Univ Rennes, École Nationale Supérieure de Chimie de Rennes, CNRS, ISCR (UMR 6226, F-35000 Rennes, France

[d] Higher Institute of Applied Sciences and Technology of Gabes, University of Gabes, Tunisia

* Corresponding authors. E-mail: aymen.assadi@ensc-rennes.fr (A.A. Assadi).

Abstract

In this paper, a Reed-based composite (R) beads, combined with photocatalysis, for the oxidative degradation of fluoroquinolones ciprofloxacin (CIP) in simulated hospital wastewater was developed. It is well known that hospital effluents present very diluted pollution (less than 5 mg/L), The first purpose, which concerns the first step to treat CIP solution (4 mg/L) via adsorption on (R) beads in continuous column system. The second aim was to regenerate the material for the simultaneous R reuse and CIP desorption in a low volume of a highly concentrated solution (≈30 mg/L). The third purpose was to degrade the concentrated solution of antibiotic using continuous and batch photocatalytic reactors. After CIP uptake on R-beads, two acid solutions

were investigated for the regeneration step. Indeed desorption process was investigated using acetic acid (0.1 M) and hydrochloric acid (0.1 M) as eluents, leading to a highly concentrated CIP solution (≈30 mg/L) compared to the feed solution (4 mg/L). Consequently, these results provide new study into the application of sequential combination to effectively mineralize antibiotics with continuous treatment.

Keywords: Reed-based composite (R) beads; Adsorption; regeneration; photocatalysis; Antibiotic removal.

1 Introduction

Recently, the pharmaceutical industries development and the increasing production of several antibiotics have resulted in the discharge of a large amount of hospital effluents into the water environment [1] . Ciprofloxacin (CIP) is one of the most used synthetic antibiotics. Because of its antibacterial activity, CIP is excessively applied to clinical medical treatment [2]. This antibiotic is broadly present in water sources owing to incomplete metabolism in humans, or coming from effluents of drug production industries [3]. CIP is not easily biodegradable [4]. However, owing to its recalcitrant character to microbial degradation, CIP is frequently detected in aquatic environment, often at low concentration [2]. The CIP concentration has been measured in wastewater influents, effluents and streams to be less than 1 µg/L. However, higher CIP concentrations have been found in hospitals effluents (between 3 and 87 µg/L), and drug manufacturers (31 mg/L) [5].

It is well-known that hospital effluents present very diluted pollution. Conventional treatment using a single process such as photocatalysis or adsorption will not be effective of a continuous removal.

Many previous studies deal with CIP concentrated solutions removal, including adsorption [5], photodegradation [2], oxidation [6], electro-Fenton [7] and ozonation processes [8]. The complexity of treatment is linked to the specificity of the CIP effluent, which are characterized by large volumes at low concentrations of antibiotics. The primary idea of the present study was to concentrate this effluent in a small volume, which can be then easily and efficiently treated by advanced-oxidation-processes (PAO) like photocatalysis. This should allow a significant mass transfer between the bulk and the catalyst phases inducing efficient oxidation

Antibiotic has several toxic effects on human being, such as vomiting, leucopenia and stomatitis [9]. Therefore, its amount in wastewater must be reduced to an admissible level before being spilled in drainage system. There is a lack of studies carried out on the CIP removal, when compared with other antibiotics. CIP structure has a planar configuration as illustrated in Fig. S1. The values of pKa for CIP are 5.90 ± 0.15 (carboxylic acid group) and 8.89 ± 0.11 (basic-N-moiety) [10]. Consequently, CIP molecules can have an anionic, zwitterionic and cationic form, depending on the water pH value, (Fig. S1) [5].

The current trend is to move towards a combined system. The idea is that the adsorption part pollution scavenging in small volume and the photocatalysis ensured a treatment of a concentrated solution issued form adsorption part. It is noted that photocatalysis exhibits weaknesses during the diluted-solutions treatment because of the limitation of pollutant transfer of the material from the liquid-phase to the particles of titanium dioxide. Thus, treating concentrated solution can be interesting with photocatalysis process [11].

In this work, synergetic loading-regeneration-photocatalysis, was performed to eliminate CIP existing in wastewater at low concentration. The loading step took place in two phases. The first one consisted in antibiotic removal from the effluent. It was performed in column, using Reed (*Phragmites australis*) lignocellulosic material, as an invasive plant that is found extensively in wet area in the Gabes region (Tunisia). The second step, the regeneration process, was then realized to recover the eliminated CIP in a highly concentrated solution. The third step of the process was the photocatalysis of the CIP contained in this latter solution. To our knowledge, no sequential combination between a desorption process based on low-cost material with an oxidation process was investigated for the continuous treatment of antibiotics.

2 Materials and Methods

2.1 Chemicals

Ciprofloxacin ($C_{17}H_{18}FN_3O_3$, wt=331.34 g/mol) and 1-Butyl-3-methylimidazolium chlorides (BMIMCl) were respectively purchased from Sigma Aldrich and abcr GmbH and used without supplementary purification. Stock solution of CIP (50 mg/L) was prepared by mixing 50 mg of antibiotic and 1 L of ultra-pure water. Then, the working concentrations were daily prepared by suitable dilution. Ultra-pure water was utilized during the investigation.

2.2 Bio-beads preparation

To eliminate the antibiotic from wastewater, lignocellulosic biocomposite beads (referred to as R) may be prepared using reed, which is an invasive plant that is found extensively in marshes in the Gabes region (Tunisia). The biocomposite synthesis protocol is inspired by the Karoui et al.'s protocol [12], as follows: the reed

was cleaned, dried and sieved so as to prepare the reed powder. R-beads are composites of equal quantities of two compounds (R_1 and R_2). On the one hand, the reed powder was treated using an orthophosphoric acid (H_3PO_4) solution (1 M). The obtained mixture was neutralized until pH = 7.0 ± 0.1, and the dough was carbonized at 250 °C to obtain the first compound (R_1). On the other hand, the reed was dissolved in BMIMCl to obtain R_2, then the R_1 was added [12,13]. The homogeneous and viscous obtained mixture was added dropwise into a distilled water bath using a 3 mm diameter pipette.

The obtained beads were then rinsed with distilled water until disappearance of BMIMCl (control made by pH and conductivity measurements). Finally, the beads were frozen at T= -17 °C, to prepare them for lyophilization. The synthesized R-beads were stocked in desiccators for further use.

2.3 Characterization methods

Fourier-Transform-Infrared Spectroscopy (FTIR) was performed to define the chemical compositions of R-beads and the catalyst. The changes in the surface chemistry of R, after the CIP uptake, and that of the TiO_2 catalyst after photodegradation were also examined by FTIR. PerkinElmer, USA, Spectrum Two FTIR spectrometer with an Attenuated-Total-Reflectance (ATR) crystal accessory (diamond) was utilized to obtain all spectra. For each spectrum, four scans were carried out at a resolution of 2 cm^{-1} with the wave-number range from 4000 to 450 cm^{-1}. Measurements were performed by a Deuterated-Glycine-Sulfate (DTGS) detector.

The characterization of surface morphologies of R-beads and the catalyst before and after treatments was performed using Scanning-Electron-Microscopy (SEM, IT 300).

2.4 Analytical methods

The quantification of CIP in the solutions was performed by an UV-visible spectrophotometry (Cary 50 probe, Varian) at 273 nm.

The percentage antibiotic removal (%R) and the loaded amount onto the R-beads at equilibrium (q_e) were calculated using Eq. (1) and Eq. (2), respectively [14].

$$q_e = \frac{(C_0 - C_e)V}{m} \quad (1)$$

$$\%R = 100\frac{(C_0 - C_e)}{C_0} \quad (2)$$

Where C_0 and C_e are the initial and the equilibrium concentrations (mg/L), respectively. V is the solution volume (L). m is the mass of R (g).

The organic matter in suspensions was quantified by a Shimadzu A-200 Total-Organic-Carbon (TOC) analyzer (Tokyo, Japan).

The percentage of TOC removal (%TOC) during the photo-degradation was calculated using the following equation [1] :

$$\%TOC = 100\frac{(TOC_0 - TOC_t)}{TOC_0} \quad (3)$$

Where, TOC_0 and TOC_t are the organic content (mg/L) in initial state and at time t, respectively.

The desorption efficiency was determined using Eq. (4)

$$\text{desorption efficiency} = \frac{\text{Amount of recovered CIP}}{\text{Amount of eliminated CIP}} \times 100 \quad (4)$$

2.5 Uptake process

The CIP uptake from wastewater was performed in a fixed-bed column. Fig. S2 shows the schematic model of the experimental semi-pilot. The height and the internal diameter of the used bed were 0.12 m and 3 cm, respectively. An amount of 6 g of R-beads was packed up in the fixed-bed, which was mounted vertically. Grids were placed at the top and the bottom end of the bed to keep the R-beads inside the column. A CIP solution was passed through the column after fixing the flow rate. The pump (Cole-Parmer, Illinois, USA) was used to control the flow rate and facilitate the liquid flow through the fixed-bed. The effect of the feed-concentration and that of the flow-rate on the CIP removal were studied. All experiments were performed at room temperature (20 ±1 °C) and the natural CIP pH, 7.32.

2.6 Regeneration Step

The continuous desorption experiments were performed in the same semi-pilot (Fig. S2) by replacing the CIP with the eluent. In this work, two eluents were used, which were acetic acid (CH_3COOH, 0.1M) and hydrochloric acid (HCl, 0.1M). Experiments were released at T = 20 ±1 °C and with flow-rate of 1 L/h. The recovered solutions obtained using acetic acid (RS-AA) and hydrochloric acid (RS-HA) were then treated by photocatalysis.

2.7 Photocatalytic treatment

For photocatalysis experiments, titanium dioxide (TiO_2) deposited on cellulosic paper was utilized as a catalyst. The preparation procedure of this catalyst was already described by Assadi et al. [15]. A dry mixture of 50 wt% TiO_2 nanoparticles (PC500, Millennium) and 50 wt% colloidal silica was suspended in ultrapure water. A suspension composed of 40% dry powder and 60% ultrapure water was prepared to ensure the coating of 13 g/m^2 of dry TiO_2 on the cellulosic support. The press was

utilized to impregnate the paper with the suspension. Then, the obtained cellulosic paper was dried in an oven at T=105 °C and then stored in rolls for ulterior use.

The antibiotic photocatalytic degradation was performed in continuous using a falling film reactor (Fig. S3) and in batch reactor (Fig. S4). Indeed Fig. S3 shows the used semi-pilot, which consisted in a six steps stainless steel falling film photoreactor. The presence of 6 steps of staircase allows increasing the surface catalytic material surface and improves the oxygenation of the treated solution. In fact, the catalytic film geometry allows increasing the exchange surface between the antibiotic solution and the air; consequently, the oxygen transfer in the liquid-phase increases. A catalyst of 0.20 m^2 (78 cm*26 cm) surface was used. Three UV-A lamps (36 mW/cm^2, Philips Netherlands), placed under the lid, delivered a spectral emission at a wavelength of 365 nm for each lamp. The recovered CIP solution was introduced in a glass vessel of volume 2 L. The peristaltic electro pump was utilized to inject the solution from the solution tank, under continuous stirring. A thin liquid film on the TiO_2 catalyst generates a low UV light absorption. The effect of the flow-rate and that of the UV-light-intensity on the CIP degradation were examined. Moreover, CIP degradation in batch reactor (Fig. S4) was carried out in a glass reactor of 1L capacity, in the presence of an UV-A lamp (12 mW/cm^2, Philips Netherlands), with a spectral emission of 365 nm. For each experiment, 1 L of recovered CIP wastewater and 0.05 m^2 of catalytic material (31.5 cm x 16 cm) surface were added in the reactor. The tube containing the lamp was immersed in the middle of the reaction solution.

3 Results and Discussion

3.1 Characterization of the materials

The baseline and the normalization of spectra of R before and after CIP uptake were performed using Origin 8.5 software (Fig. 1). The broad band of C–H and O–H stretching vibrations within the 3650-3000 cm^{-1} region observed in both spectra showed the principal functional groups found in lignocellulosic materials [16]. An increase of these peaks intensities was observed after CIP uptake. This can be related to the presence of C–H, O–H and N-H groups in the CIP molecules. The signal at 2920 cm^{-1} can be related to symmetric C-H vibrations in cellulose and hemicelluloses [17]. The observed peak at 2850 cm^{-1} was due to C-H stretching in lignin [18]. Both spectra show another intense peak at 1711 cm^{-1}, which was related to the C=O and CO_2 elongation vibration, and would be obtained by transformation of ketones, phenols, ether, esters and/or aromatic carboxylic groups [19]. The signal within 1580-1620 cm^{-1} in the two spectra can be attributed to C=C in plane aromatic vibrations, and C=N bond [20], indicating the CIP presence. Moreover, lignin showed characteristic band within 1517-1505 cm^{-1} originating from C=C aromatic vibration. After CIP uptake, an increase in intensities of peaks at 1711, 1600, 1517-1505 cm^{-1} was observed. This can be related to the presence of C=O elongation and C=C aromatic vibrations, which confirms the CIP adsorption on R-particles. Similarly, after CIP uptake, increase of intensities of bands at 1372 cm^{-1}, 1315 cm^{-1} and 1229 cm^{-1} assigned to the C-C deformation, O-H and CH_2 stretching and C-C band respectively, were observed [21,22].

After CIP uptake on the R surface, the bands at 1454 cm^{-1} and 1232 cm^{-1}, associated to the C-H deformation vibrations [23] and C-O bonds [24] shifted to 1457 cm^{-1} and 1237 cm^{-1}, with an increase in peaks intensities, respectively. Similarly, the band at 1046 cm^{-1} and 898 cm^{-1} related to the C-F bond, C-O-C bond [25] of the cyclic alcohol of cellulose and C-H deformation vibrations of cellulose switched to 1041 cm^{-}

^{1} and 895 cm^{-1}, respectively, with a slight increase in peaks intensities. The observed band shifts and transmittance increase can be explained by the formation of intermolecular hydrogen-bonds between particles, which would confirm the CIP adsorption on R-particles. Similarly, the appearance of new groups characteristic of the CIP molecule at 1337 cm^{-1} and 749-832 cm^{-1} in the R-CIP spectra could be ascribed to the N=O bond and C-H aromatic vibrations, respectively, which would confirm once again the presence of the CIP molecules on the R surface.

The FTIR characterization was performed so as to emphasize the heterogeneous characteristic of the catalyst surface and highlight the existence of several functional groups such as carbonyl, hydroxyl, carboxylic and phenolic groups. After experiments of antibiotic degradation in different systems, (i.e., (c) CIP in ultra-pure water, (e) CIP in RS-AA and (f) CIP in RS-HA), photocatalysts were recovered from the reactor, and analyzed by FTIR (Fig. 1d, e and f). A large band observed between 3000 cm^{-1} and 3600 cm^{-1} in the raw catalyst spectra (Fig. 1c) attributed to O-H groups, indicated the presence of polysaccharides and cellulose molecules on the photocatalyst surface [26]. Increases of this band intensities band were observed on all spectra of catalyst after CIP degradation in various medium. This can be related the deposition of antibiotic molecules and their by-products onto the catalyst surface. As was confirmed by [7,27,28] all CIP photocatalysis degradation by-products contain OH groups. By comparing the band attributed to O-H groups in the three FTIR spectra (Fig. 1c, d and e) of catalyst, one can observe that its intensity went up after CIP degradation in RS-HA (spectrum in Fig. 1f)**.** Indeed, a higher OH band intensity on the latter spectrum may indicate a low CIP degradation efficiency in HA medium due to low by-products generation (responsible of OH band intensification).

The raw catalyst spectra show series of peaks within 2928-2868 cm^{-1} representing the spectrum bands of C-H vibrations, indicators of methyl (-CH_3) and methylene (-CH_2) groups. After CIP degradation in acid solution, this band was compressed from 2928-2868 cm^{-1} to 2922-2950 cm^{-1} suggesting the involvement of C-H vibrations in the retention of CIP antibiotic molecules and their by-products [29]. In addition, this peak series has the lowest intensity in the FTIR spectrum (Fig. 1d). In fact, a lower C-H band intensity on the latter spectrum may indicate a high CIP degradation efficiency in ultra-pure water medium.

Carbonyl (C=O) stretch were recorded at 1734 cm^{-1}, corresponding to aldehyde and ester groups. An increase of this band intensity was observed in the FTIR spectrum in (Fig. 1e). This can be related to the fixation of antibiotic molecules onto the catalyst surface. Indeed, a higher C=O band intensity on the latter spectrum may indicate a low CIP degradation efficiency in AA medium compared to CIP degradation efficiency in ultra-pure water due to low by-products generation (responsible of C=O band intensification). Decrease of the intensity of C=O band at 1734 cm^{-1} was observed in spectra in ultra-pure water (Fig. 1d), which could be attributed to the neutralization of the functional groups, and their involvement in the fixation of antibiotic molecules. The carboxylic (COO^-) stretching characterizing primary and secondary alcohols, ether and aliphatic groups were observed at 1635 cm^{-1} [30]. Decreases of this peak intensities were observed on the three FTIR spectra of catalyst after CIP degradation. This may be related to the transformation of COO^- groups to CO_2 groups according to the photo-kolbe reaction [31]. The same signal was observed in the spectra in Fig. 1d**,** with higher intensity, and in Fig. 1e, with lower intensity caused by the neutralization of the functional groups, and their potential involvement in the antibiotic molecules uptake onto the catalyst surface. Ester stretching (C-O) were found

between 1370 cm^{-1} and 1313 cm^{-1} [29]. The spectra of catalyst after CIP degradation in RS-AA solution shows an increase of intensity of the C-O peaks, confirming the presence of C-O groups, which would suggest the CIP antibiotic uptake onto the catalyst surface. The observed stretching at 1057 cm^{-1} and 896 cm^{-1} represented the C-O-C bond of the cyclic alcohol of cellulose [32]. An increase in the C-O peak was observed in the spectra of catalyst after CIP degradation in ultrapure-water (Fig. 1d) and RS-AA (Fig. 1e), through the shifts from 1057 cm^{-1} to 1059 cm^{-1} and to 1053 cm^{-1} respectively. In addition, FTIR curve of the TiO_2 catalyst after antibiotic injection in RS-HA showed a transmittance increase at 1057 cm^{-1}. The same behavior was noticed after CIP degradation in various solutions, for C-O-C groups at 896 cm^{-1}. The band deviations confirmed the involvement of functional groups in the retention of CIP by-product antibiotic. Peak at 796 cm^{-1} is often attributed to amine groups [33]. A transmittance increase was observed at 796 cm^{-1} in the spectrum in Fig. 1f, confirming the presence of CIP by-products on the catalyst surface.

Ester stretching (C-O) were found between 1370 cm^{-1} and 1313 cm^{-1} [29]. The spectra of catalyst after CIP degradation in RS-AA (Fig. 1e) solution shows an increase of intensity of the C-O peaks, which would suggest the deposition onto the TiO_2 catalyst surface of photocatalytic by-products of the CIP molecules.

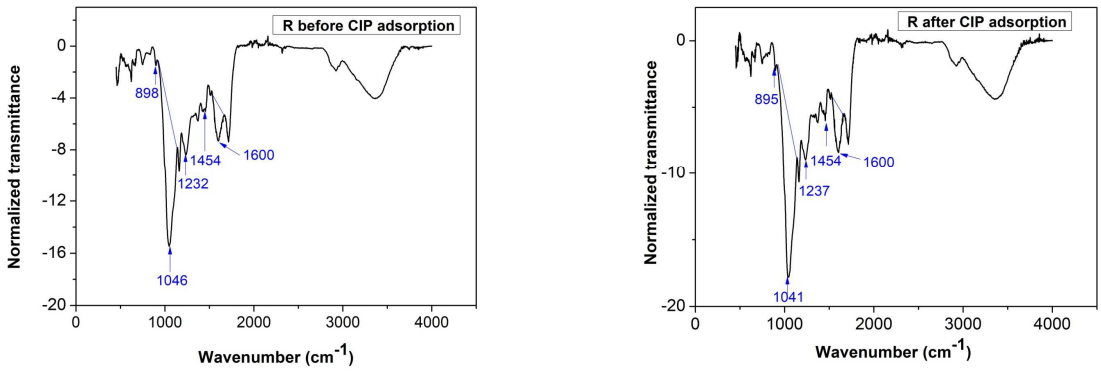

Fig.1a

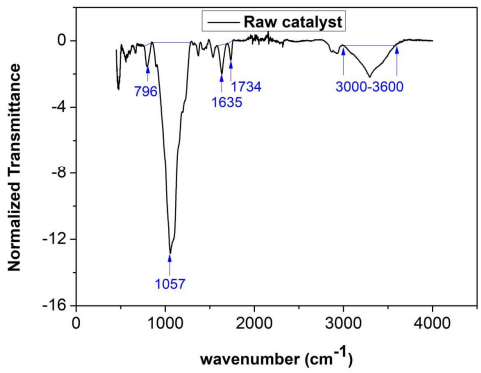

Fig.1b

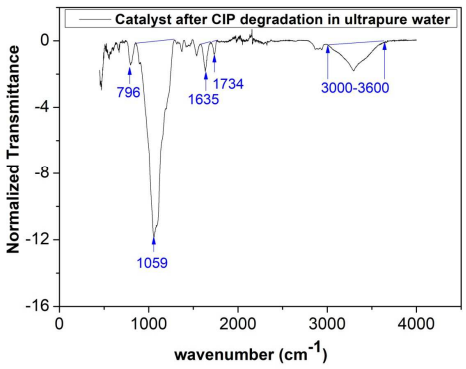

Fig.1c

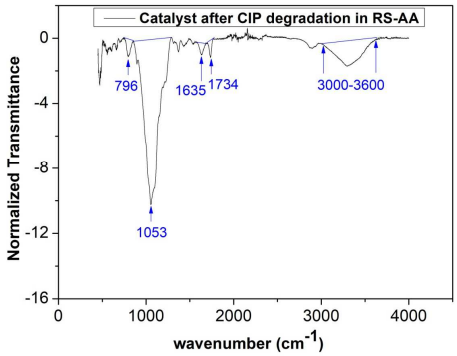

Fig.1d

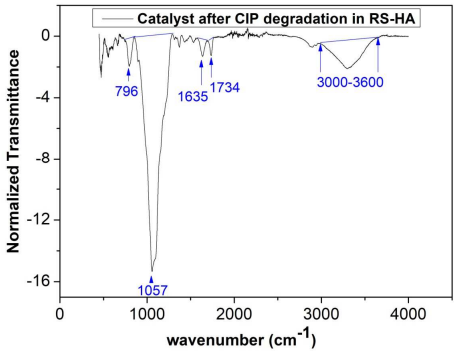

Fig.1e

Fig.1f

Fig. 1. FTIR curves of (a) R-beads and (b) R-beads loaded with CIP; FTIR curves of (c) Raw catalyst and catalyst after photodegradation of CIP in (d) ultra-pure water, (e) RS-AA and (f) RS-HA.

Figures 2a, b, c and d show the porosity of R surface through SEM micrographs of R surface before and after antibiotic uptake. Fig. 2a-b exhibits a clear sight of the pores at R surface. Similarly, the SEM micrograph of R revealed a porous and rough surface and an irregular structure. The surface morphology of R appeared to have an uneven-structure and porous-cavities. With these features the surface morphology of R can be deemed very-adequate as an active-site for the CIP contaminant. However, the SEM micrograph of R-CIP beads (Fig. 2c-d), shows that many particles were

dispersed on the beads surface, which was ascribed to the coverage of R surfaces by CIP molecular species. In addition, Fig. 2c-d discloses that the clear pore textural structure is not observed on the surface of R after adsorption process which could be due to the incursion of CIP molecular species into the pores of R [34]. Figures 2e, f, g and h illustrate the porosity surface of the used catalyst through SEM images. SEM imaging of raw catalyst (Fig. 2e) showed that this photocatalyst is characterized by an important porosity, which allows pollutants molecules to be adsorbed onto its surface. Moreover, SEM images an equal distribution of TiO_2 powder on the cellulosic paper surface which would permits a homogeneous liberation of free oxidizing radicals on the catalytic surface under UV-radiation. After aqueous-solutions of CIP inlet, SEM images presented a homogeneous morphologies with equal partition of spheres proving the CIP antibiotic molecules deposition onto the catalyst [29] (Fig. 2f, g, h)**.** Besides, the SEM micrograph of catalyst after CIP degradation, showed that the surface became rougher compared to catalyst surface morphology, indicating the disposition of CIP molecular species and their degradation by-products on the surface.

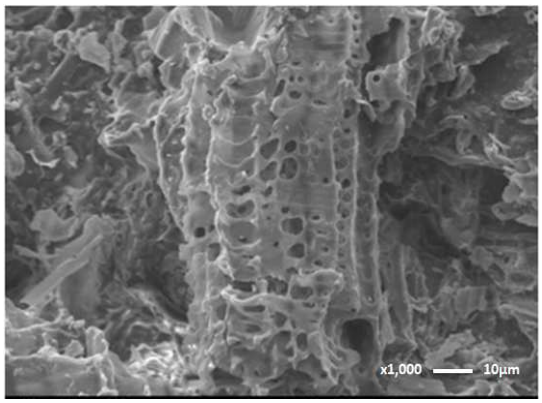

Fig.2a

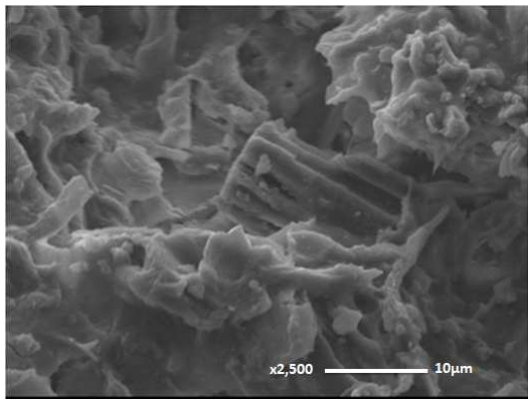

Fig.2b

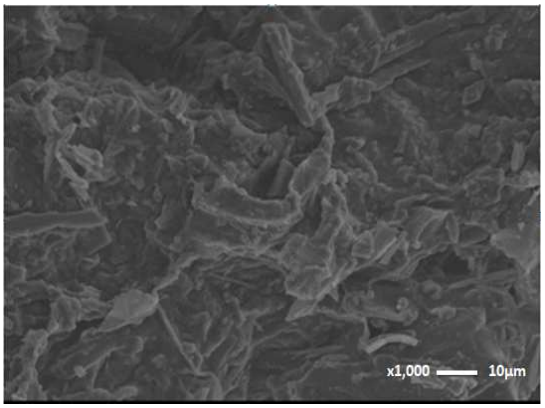

Fig.2c

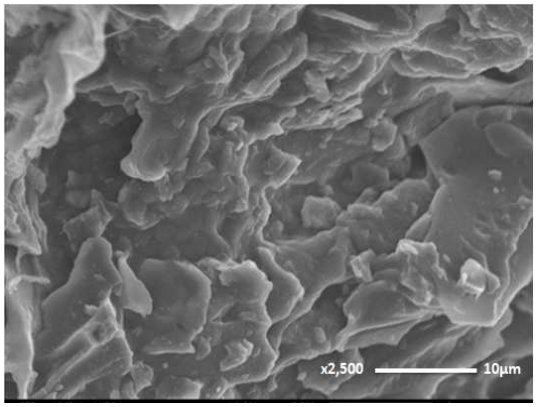

Fig.2d

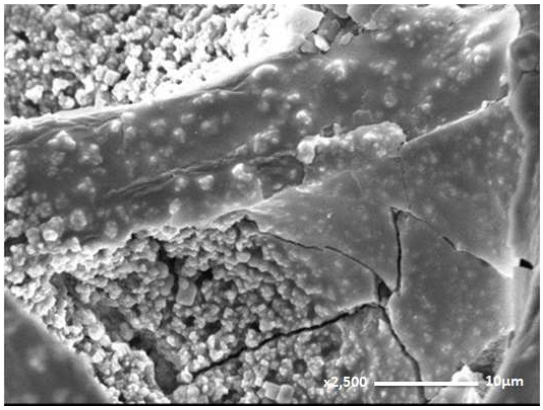

Fig.2e

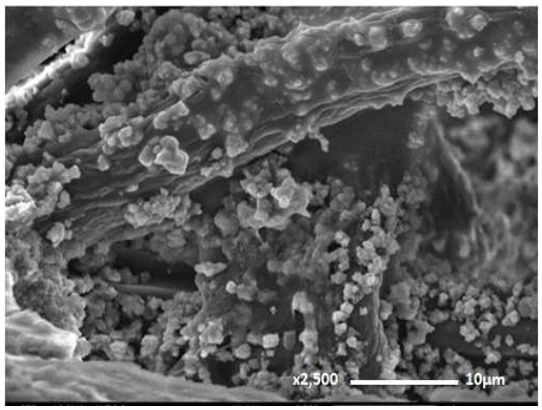

Fig.2.f

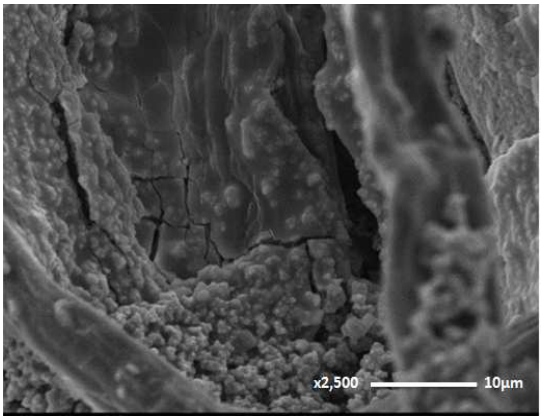

Fig.2g

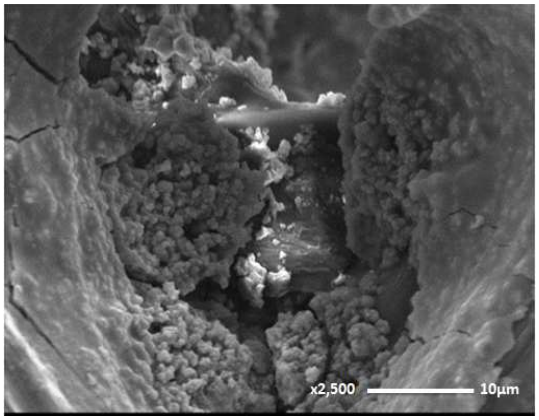

Fig.2h

Fig. 2. SEM images of R surface: (a-b) SEM images of R before uptake, (c-d) SEM images of R after CIP uptake; SEM images of the catalyst: (e) raw catalyst, (f) catalyst after CIP photodegradation in ultra-pure water, (g) catalyst after CIP photodegradation in RS-AA, (h) catalyst after CIP photodegradation in RS-HA .

Moreover, the chemical-composition of the photocatalyst before and after degradation was studied by EDX analysis from which the presence of Al, Ti, Si, O, and C in the samples was confirmed (Fig. S5a-d). The Al peak observed in the EDX-pattern is related to aluminum coated for SEM image acquisition. The Ti and Si peaks observed in the EDX-patterns are related to catalyst surface, which is a titanium dioxide (TiO_2) deposited on cellulosic paper. This catalyst was prepared from a dry mixture of 50 wt% TiO_2 nanoparticles and 50 wt% colloidal silica. In the Fig. S5 (EDX analysis) C and O are the dominant elements throughout the photocatalyst surface with weight percentages of 27.58% and 50.37%, respectively for the raw catalyst (Table 1).

Element	Weight (%)			
	Raw catalyst	Catalyst after CIP degradation in ultrapure-water	Catalyst after CIP degradation in RS-AA	Catalyst after CIP degradation in RS-HA
Al	0.93	0.41	1.68	-
C	27.58	27.41	24.25	24.99
O	50.37	50.65	50.90	52.13
Si	11.69	12.56	12.68	12.93
Ti	9.43	8.97	10.49	9.95

Table. 1 Elemental compositions of catalysts obtained by EDX

The weight percentage of Carbon in the photocatalyst surface decreases to be 27.41, 24.25 and 24.99% (Table 1) after CIP degradation in ultrapure water, in RS-AA and RS-HA suggesting the involvement of Carbon atoms in the retention of CIP molecules and their by-products. This finding is in good agreement with the FTIR results.

3.2 CIP elimination

3.2.1 Effect of the flow-rate

The CIP removal in column was studied with various flow-rates in the range of 0.5-3 L/h, as illustrated in Fig. 3a**.** For the six flow rates, the percentages CIP removal was determined, by passing 1.5 L of antibiotic solution with a concentration of 4 mg/L through the fixed-bed during 1.5 h. The removal percentage decreased from 91.62 % to 55.07 %, and the number of recycling cycles increased from 0.5 to 3, as the flow-rate increases from 0.5 to 3L/h, respectively. This result proves that the efficiency of the CIP removal process decreased with the increasing of flow-rates, which can be related to the presence of more non-saturated active site. Moreover, the increase of flow-rate should allow more turbulence on the fixed bed surface, reducing the resistance to the external mass-transfer of CIP. In addition, the recycling cycles number decreased at lower flow-rate [35].

3.2.2 Effect of the feed concentration

To study the effect of the CIP antibiotic concentration on the elimination process, various inlet initial CIP concentrations from 4 to 8 mg/L were investigated with the same flow-rate of 1 L/h and a volume of 1.5 L of CIP solution. The initial CIP concentration had an important influence on the CIP removal capacity as illustrated in Fig. 3b. The eliminated amount of antibiotic increased from 0.76 to 1.52 mg/g as the initial feed concentration of CIP increased from 4 to 8 mg/L, respectively. This result proves that the change of concentration-gradient can affect the saturation rate, the breakthrough time and the diffusion procedure. The CIP loading rate increased with increasing the feed concentration, due to a decrease of the mass-transfer force for a fixed sorption bed length [36]. In addition, the high feed concentration of antibiotic

provides the concentration-gradient for the mass-transfer process and hence a higher amount of antibiotic can be eliminated from the solution, resulting in an increasing of the breakthrough time. Moreover, a higher concentration-gradient engenders an increase in the diffusion coefficient and leads to a faster transport of CIP from the antibiotic on the R-beads and an earlier breakthrough time. Therefore, higher column performances can be reached for higher initial concentration in the solution [37]. However, in this work the subsequent-experiments were performed with an initial CIP concentration of 4 mg/L for the simple reason that the CIP concentration in wastewater is very low.

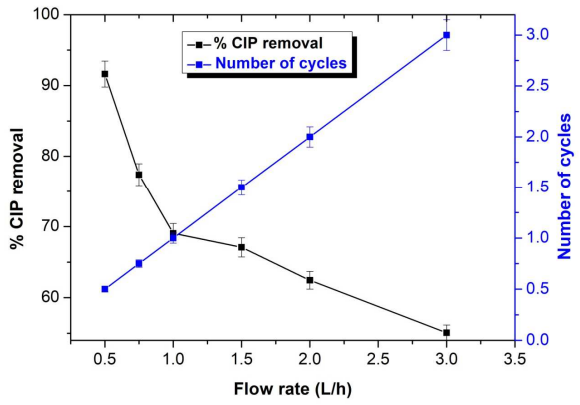

Fig.3a

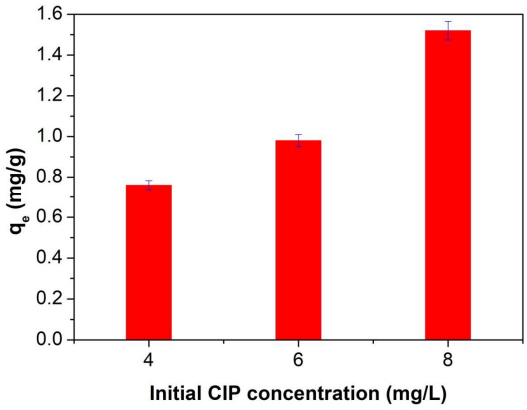

Fig.3b

Fig. 3. (a) Effect of the flow-rate on the CIP removal (CIP initial concentration = 4 mg/L Time = 1.5 h, Volume = 1.5 L); (b) Effect of the feed-concentration on the CIP removal (flow rate = 1 L/h Time = 1.5 h, Volume = 1.5 L)

3.2.3 Column removal capacity

During the experiments, the feed-concentration and the flow-rate were maintained at constant values of 1 L/h and 4 mg/L, respectively. Fig. S6 shows the obtained breakthrough-curves for two cycles. **Table 2** illustrates the column uptake capacity at

100% breakthrough for CIP on the R-beads for two cycles. The breakthrough was calculated using the following equation:

$$\text{Breakthrough}\ (\%) = \frac{C}{C_i} \times 100 \qquad (5)$$

where C_i and C are the inlet and the outlet concentrations of antibiotic (mg/L), respectively. 100% of breakthrough means that $C=C_i$; thus the material saturation was reached.

100% breakthrough ($C=C_0$)	First cycle	Second cycle
q_e (mg/g)	59.92	27.89
Volume of treated solution (L)	164	99

Table. 2 Experimental data for column parameters calculated at inlet-concentration of 4 mg/L, and flow-rate of 1 L/h, for two cycles.

The column capacity for CIP uptake for a column height of 0.12 m and for 100% breakthrough were found to be 59.92 mg/g and 27.89 mg/g for the first and the second cycle, respectively. The R-beads and the used column led to the CIP removal from a solution volume of 164 L and 99 L for the first and the second cycle, respectively.

The pH_{pzc} of R-beads is 4.8. The removal experiments were released at the natural pH of CIP, which was equal to 7.32. At this pH, the CIP exists in a zwitterionic form (CIP^{+-}, Fig. S1.) and the R-material is negatively-charged. The CIP elimination phenomenon resulted therefore from the electrostatic attraction between the antibiotic and the R-beads surface, explained the high uptake efficiency. In addition, the CIP uptake may be controlled by hydrophobic interactions and/or the π-π stacking interaction.

3.3 Regeneration study

The cost effectiveness of a material depends on its reusability, which reduces the cost of the uptake process. The loading and regeneration cycles were repeated two times. To recover the CIP, desorption-experiments were performed using acetic acid (0.1 M) and hydrochloric acid (0.1 M) solutions for the first and the second cycle, respectively. Using CH_3COOH and HCl, up to 61.74% and 48.41% of the CIP were recovered from the loaded biocomposite beads, respectively, after 33 hours (Fig. 4). The reuse of the R-beads confirms that the process is economical and efficient. The desorption efficiency by CH_3COOH and/or HCl can be explained by the electrostatic repulsion between the R-beads (pH_{zpc}=4.8) and the CIP-molecules which were both positively-charged in acidic solution [38].

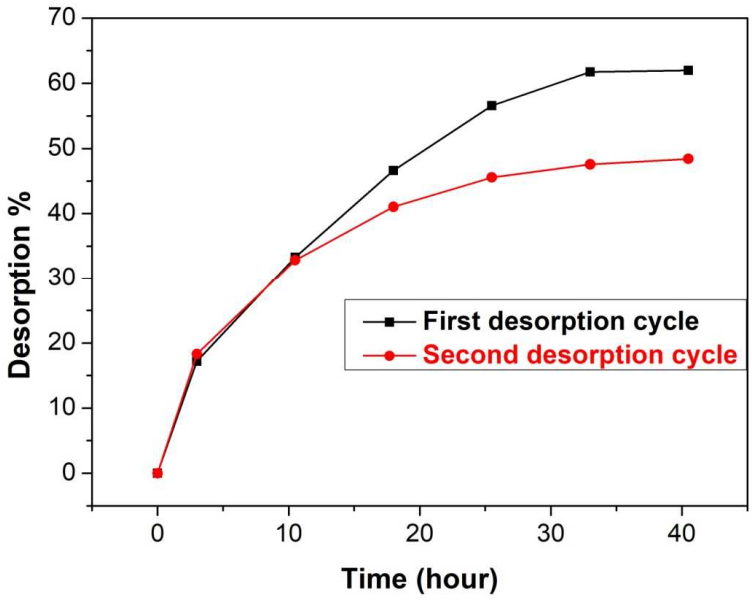

Fig. 4. Kinetics of desorption

Using the loading-regeneration process, solutions of 31.71 mg/L and 29.52 mg/L were recovered, for the first and the second cycle, respectively. Acetic acid and/or

hydrochloric acid as eluent allowed the simultaneous regeneration of the material and the desorption of the CIP antibiotic in a highly concentrated solution (≈30 mg/L) compared to the feed solution (4 mg/L). The recovered solutions obtained using acetic acid (RS-AA) and hydrochloric acid (RS-HA) were then treated by photocatalysis. It is therefore clear that the loading-regeneration process allowed generating solutions of volume 7 L and 5 L instead of solutions of volume 164 L and 99 L.

3.4 Photocatalysis degradation: Continuous mode

3.4.1 Effect of the flow-rate

Photodegradation of the CIP contained in the RS-AA solution was investigated in the falling-film closed loop step photoreactor at pilot scale. Here the photocatalytic-performance was investigated at various flow-rates. The RS-AA solution was chosen, owing to the high amount of solution available (7 L – see 3.3). The examined flow-rates of the effluent were 47, 80, and 102 L/h. Figure. 5. shows the influence of the effluent flow-rate on the CIP degradation and mineralization. It can be seen that the flow-rate had only a slight but signification impact on the mineralization; while the impact on the degradation yield appeared almost negligible. At higher flow-rate, two phenomena may happen; the improvement of the mass-transfer and the reduction of the residence time. Consequently, the overall kinetics reaction would thus be completely controlled by the mass transfer step [39]. Therefore, this behavior can be explained by the fact that when the water film is thin, oxygen adsorption onto the catalytic surface leading to reactive-oxygen-species (ROS) generation is improved. Moreover, this technology of falling-film enhances the photon entering into the interface between the two phases leading to more e/hole formation.

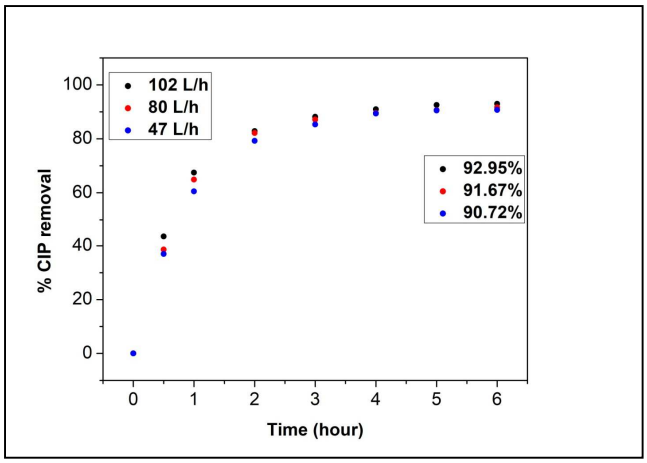

Fig. 5a

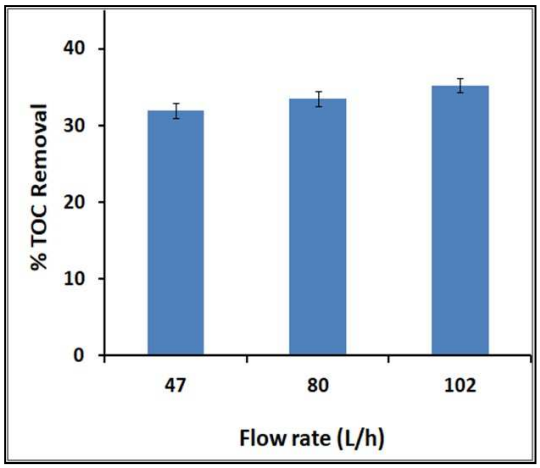

Fig.5b

Fig. 5. Effect of the flow-rate on (a) CIP degradation and (b) TOC removal (C_0≈30 mg/L).

Figure. S7. Shows the comparaison of kinetic of desorption and that of photodegradation. It was observed that the photodegradation process (4 hours) is faster than the desorption process (33 hours), which confirm the efficiency of photodegradation process.

3.4.2 Effect of UV-light intensity

Heterogeneous degradation of the CIP contained in the RS-HA solution was performed in the falling-film closed loop step photoreactor under various UV-light intensities. The examined intensities were 12 mW/cm^2 using one lamp and 36 mW/cm^2 using three lamps. Figure. S8**.** shows the removal capacity dependency on the light irradiation intensity. Accordingly, it is known that UV-light intensity is an important factor for the application of TiO_2 photocatalytic method for cleaning wastewater [40]. The results indicated that an increase in the irradiation intensity enhanced the antibiotic removal. Under higher UV-light intensity, the formation of electron–hole is predominant, and hence the recombination of electron–hole is

negligible. While, at low light intensity, it is well known that there is competition between separation and recombination of electron–hole pair, which decreases the free radicals formation and the photodegradation efficiency of antibiotic [41].

3.5 Suggested mechanism of the CIP degradation

3.5.1 Effect of chemical composition of the irradiated matrices (pH): Batch mode

To study the influence of the composition of the reaction-medium, CIP photocatalysis experiments, in the presence of the same concentration of TiO_2, were carried out in ultrapure-water (as model matrix), tap-water (as consumed water), recovered solution by acetic acid (CIP in RS-AA) and recovered solution by hydrochloric acid (CIP in RS-HA). The results illustrated in Fig. 6a-b proved that the efficiency of the catalytic process is affected by the physicochemical quality of the dilution matrices. Indeed, CIP was degraded more rapidly in ultrapure-water than in tap-water and recovered solutions.

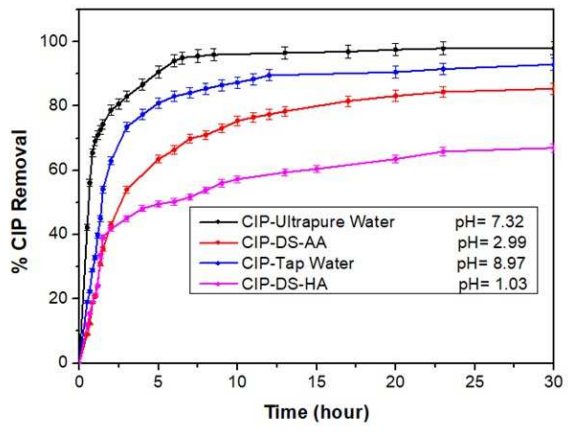

Fig.6a

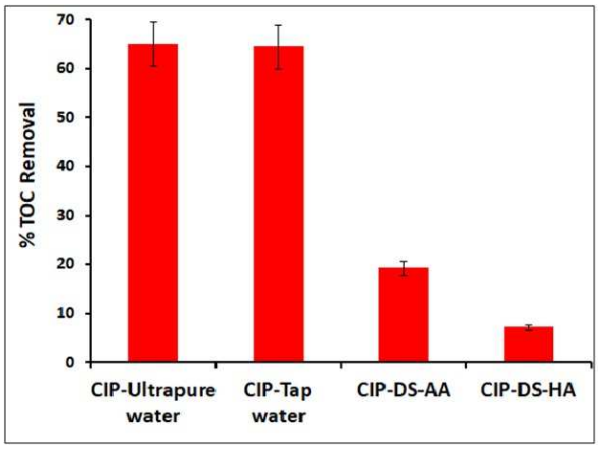

Fig.6b

Fig. 6. (a) CIP degradation and (b) TOC removal, as a function of the reaction time for various solutions (C_0≈30mg/L).

The low decrease in photodegradation efficiency of antibiotic in tap-water (CIP R% = 92.97, TOC R% = 64.56) compared to CIP in ultra-pure water (CIP R% = 96.97, TOC R% = 65.12) was probably due to the high concentration of bicarbonate ions (HCO^{3-}) in tap water which act as radical traps. Abundant HCO_3^-/CO_3^{2-} ions in tap water or organic material can trap $HO^{\cdot}$ radicals or attach to holes h^+ [42]. There is consequently a competition between the carbonates and CIP molecules to trap the hydroxyl radicals. This may reduce the photocatalytic activity and decrease the degradation rate of antibiotic as organic molecules [43].

The decrease in the photodegradation efficiency of antibiotic in acetic acid and hydrochloric acid were (CIP R% = 85.41, TOC R% = 19.25) and (CIP R% = 67.00, TOC R% = 7.22) respectively, may be caused by the pH effect. This finding confirms our previous interpretation of FTIR spectrum. In fact, pH of irradiated solution is one of the parameters that greatly affect the photodegradation rate, because the TiO_2 surface-charge depends on the change of solution pH. The pH values of CIP-ultrapure water, RS-AA and RS-HA were found to be 7.32, 2.99 and 1.03, respectively. Figure. 6 show that the photodegradation efficiency of antibiotic decreased with decreasing in solution pH. Hu et al indicated that the point of zero charge (pH_{pzc}) for TiO_2 is between 6.25 and 6.50 [44,45]. The surface of TiO_2 is therefore positively charged ($TiOH_2^+$) in acidic solutions and negatively charged (TiO^-) in alkaline solutions. Consequently, the low antibiotic and TOC removals in the recovered solutions can be related to the electrostatic repulsion between the antibiotic and the catalyst surface, which are positively charged. In addition, the higher photodegradation rate at higher pH may be related to more efficient generation of hydroxyl-radicals by TiO_2 with increasing concentration of OH^-. At the

alkaline pH values, the hydroxyl-radicals have to diffuse away and degrade the antibiotic in the solution [44].

3.5.2 Suggested mechanism of the CIP removal under UV/TiO_2

Under irradiation light with higher energy (hυ) than band gaps (Eg = 3.2 eV), the electrons of TiO_2 surface are excited to the conductive-band, leaving holes in the valence-band. $OH^{\cdot}$ radicals, formed by reaction between h^+ holes and electron donors, are well known as a strong oxidant which can decompose the CIP, as organic compound, at ambient temperature, as illustrated in the suggested mechanism in Scheme. 1. This mechanism can be described also as follow [46]:

$$TiO_2 + h\upsilon \rightarrow e^- + h^+ \quad \text{(R.1)}$$

$$h^+ + H_2O_{ads} \rightarrow TiO_2 + OH_{ads}^{\cdot} + H^+ \quad \text{(R.2)}$$

$$h^+ + OH_{ads}^- \rightarrow TiO_2 + OH_{ads}^{\cdot} \quad \text{(R.3)}$$

In the RS-AA solution, the h^+ holes can interact with the COO^-group of acetic acid, according to the photo-kolbe reaction [31]:

$$TiO_2(h)^+ + RCOO^- \rightarrow R^{\cdot} + CO_2 \quad \text{(R.4)}$$

It was also reported that the interaction between the e^- electrons and the dioxygen can form oxygen superoxide radicals, as follows [47]:

$$O_2 + e^- \rightarrow O_2^{\cdot -} \quad \text{(R.5)}$$

$$O_2^{\cdot -} + H^+ \rightarrow HO_2^{\cdot} \quad \text{(R.6)}$$

$$2HO_2^{\cdot} \rightarrow H_2O_2 + O_2 \quad \text{(R.7)}$$

$$H_2O_2 + e^- \rightarrow OH^{\cdot} + OH^- \quad \text{(R.8)}$$

$$H_2O_2 + h\upsilon \rightarrow 2OH^{\cdot} \quad \text{(R.9)}$$

The mentioned mechanisms may reduce the catalytic activity.

In tap water, there is a competition between the carbonates and the CIP antibiotic molecules to trap the hydroxyl radicals, as indicated in the following reactions [48]:

$$HCO_3^- + OH^{\cdot} \rightarrow CO_3^{-\cdot} + H_2O \quad \text{(R.10)}$$

$$CO_3^{2-} + OH^{\cdot} \rightarrow CO_3^{-\cdot} + OH^- \quad \text{(R.11)}$$

$$CIP + OH^{\cdot} \rightarrow \text{Oxidized CIP} + OH^- \quad \text{(R.12)}$$

The mentioned mechanisms may decrease the degradation rate of organic molecules, including the CIP compound [43].

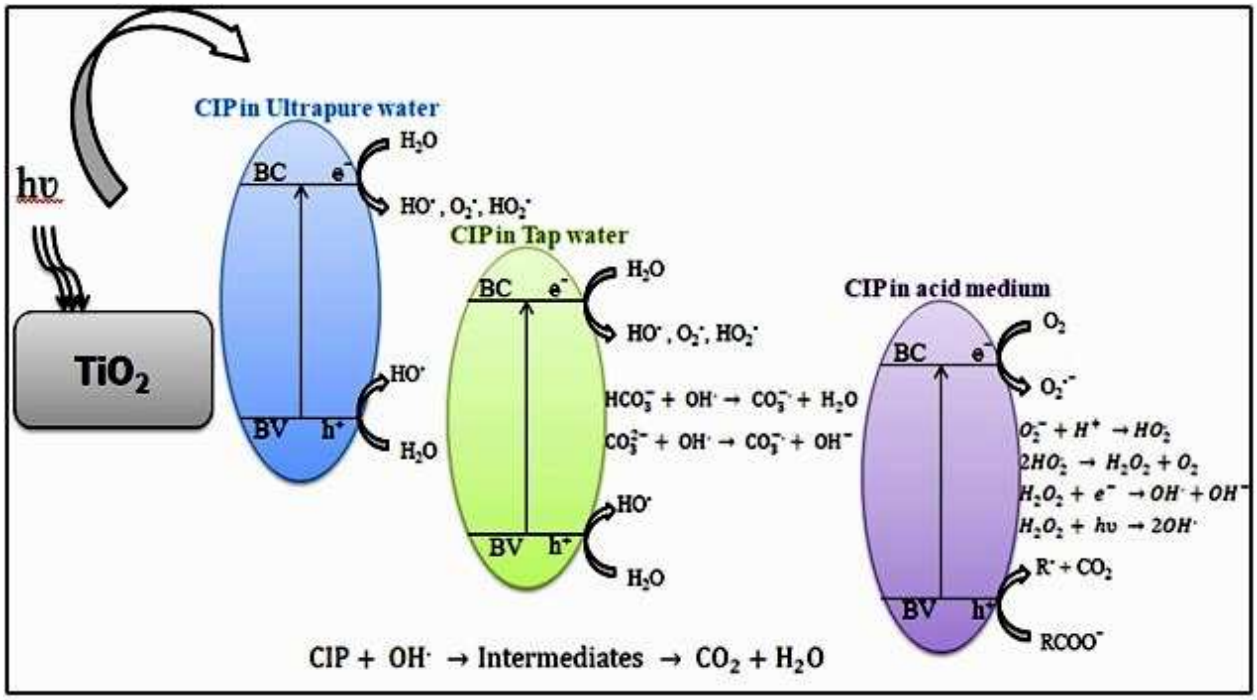

Scheme 1. Proposed photodegradation mechanism of CIP under UV/TiO_2 in various solutions.

4 Conclusion

In this work, new biocomposite beads based on lignocellulosic reed materials (R), as enhanced biomaterial, were utilized for the CIP removal from simulated of hospital effluent. The FTIR and SEM analysis of R showed the surface homogeneity. In fact, it was found that R was made of cellulose, hemicelluloses and lignin, which indicate their potential to remove antibiotic pollutant. In addition, elimination-experiments were performed to remove the antibiotic from low concentration solution (4 mg/L), using a fixed bed column. This process was efficient to treat wastewater in view of its simplicity, its high efficiency and since it is eco-friendly. Secondly, desorption study allowed the simultaneous regeneration/reuse of the material and the desorption of the CIP antibiotic in a highly concentrated solution. A CIP solution of almost 30 mg/L was obtained. Thirdly, recovered CIP solutions were well treated with semi-pilot photocatalytic falling film reactor. In this light, the results of this study (i) highlight the potential application of new biocomposites for antibiotic uptake (ii) the development of innovative sequential combination as cost-effective water technologies that can be employed to overcome the practical barriers to remove antibiotics from hospital effluents

References

[1] D. Belkheiri, F. Fourcade, F. Geneste, D. Floner, H. Aït-amar, A. Amrane, Combined process for removal of tetracycline antibiotic-Coupling pre-treatment with a nickel-modified graphite felt electrode and a biological treatment, International Biodeterioration & Biodegradation. 103 (2015) 147–153.

[2] T. Hou, H. Du, Z. Yang, Z. Tian, S. Shen, Y. Shi, W. Yang, L. Zhang, Flocculation of different types of combined contaminants of antibiotics and heavy metals by thermo-responsive flocculants with various architectures, Separation and Purification Technology. 223 (2019) 123–132. doi:10.1016/j.seppur.2019.04.068.

[3] V. Diwan, A.J. Tamhankar, R.K. Khandal, S. Sen, M. Aggarwal, Y. Marothi, R. V Iyer, K. Sundblad-tonderski, C.S.- Lundborg, Antibiotics and antibiotic-resistant bacteria in waters associated with a hospital in Ujjain, India, BMC Public Health. 414 (2010) 1471–2458.

[4] S. Wu, X. Zhao, Y. Li, C. Zhao, Q. Du, J. Sun, Y. Wang, X. Peng, Y. Xia, Z. Wang, L. Xia, Adsorption of ciprofloxacin onto biocomposite fibers of graphene oxide/calcium alginate, Chemical Engineering Journal. 230 (2013) 389–395.

[5] S.A.C. Carabineiro, T. Thavorn-Amornsri, M.F.R. Pereira, P. Serp, J.L. Figueiredo, Comparison between activated carbon, carbon xerogel and carbon nanotubes for the adsorption of the antibiotic ciprofloxacin, Catalysis Today. 186 (2012) 29–34.

[6] F. Nekouei, S. Nekouei, H. Kargarzadeh, Enhanced Adsorption and Catalytic Oxidation of Ciprofloxacin on Hierarchical CuS Hollow, Chemical Engineering Journal. (2017).

[7] H. Guo, N. Gao, W. Chu, Photochemical degradation of ciprofloxacin in UV and UV / H 2 O 2 process : kinetics , parameters , and products, Environ Sci Pollut Res. (2013) 3202–3213. doi:DOI 10.1007/s11356-012-1229-x.

[8] B. Dewitte, J.O. Dewulf, C. Links, Ozonation of Ciprofloxacin in Water : HRMS Identification of Reaction Products and Pathways, 42 (2008) 4889–4895.

[9] C.E. Cox, T.C. Marbury, W.G. Pittman, G.L. Brown, S.M. Auerbach, B.C. Fox, J.Y. Yang, P. D, A Randomized , Double-Blind , Multicenter Comparison of Gatifloxacin Versus Ciprofloxacin in the Treatment of Complicated Urinary

Tract Infection and Pyelonephritis, Clinical Therapeutics. 24 (2002) 233–236.

[10] N. Carmosini, L.S. Lee, Chemosphere Ciprofloxacin sorption by dissolved organic carbon from reference and bio-waste materials, Chemosphere. 77 (2009) 813–820.

[11] A.A. Assadi, A. Bouzaza, D. Wolbert, P. Petit, Isovaleraldehyde elimination by UV/TiO2 photocatalysis: comparative study of the process at different reactors configurations and scales. 21 (2014) 11178-11188.

[12] S. Karoui, R. Ben Arfi, K. Mougin, A. Ghorbal, A.A. Assadi, A. Amrane, Synthesis of novel biocomposite powder for simultaneous removal of hazardous ciprofloxacin and methylene blue : Central composite design , kinetic and isotherm studies using Brouer-Sotolongo family models, Journal of Hazardous Materials. (2019) 121675.

[13] S. Karoui, R. Ben Arfi, M.J. Fernández-Sanjurjo, A. Nuñez-Delgado, G. Achraf, E. Álvarez-Rodríguez, Optimization of synergistic biosorption of Oxytetracycline and Cadmium from binary mixtures on reed-based-beads : modeling study using Brouers- Sotolongo models, Environmental Science and Pollution Research. (2020). doi:10.1007/s11356-020-09493-7.

[14] M. Saad, H. Tahir, J. Khan, U. Hameed, A. Saud, Synthesis of polyaniline nanoparticles and their application for the removal of Crystal Violet dye by ultrasonicated adsorption process based on Response Surface Methodology, Ultrasonics Sonochemistry. 34 (2017) 600–608. doi:http://dx.doi.org/10.1016/j.ultsonch.2016.06.022.

[15] A.A. Assadi, A. Bouzaza, M. Lemasle, D. Wolbert, Acceleration of Trimethylamine Removal Process Under Synergistic Effect of Photocatalytic Oxidation and Surface Discharge Plasma Reactor, Canadian Journal of Chemical Engineering. 93 (2015) 1239–1246.

[16] J. Ma, Y. Lei, M.A. Khan, F. Wang, Y. Chu, W. Lei, M. Xia, S. Zhu, Adsorption properties, kinetics & thermodynamics of tetracycline on carboxymethyl-chitosan reformed montmorillonite, International Journal of Biological Macromolecules. 124 (2018) 557–567. doi:https://doi.org/10.1016/j.ijbiomac.2018.11.235.

[17] R. Ben Arfi, S. Karoui, K. Mougin, A. Ghorbal, Adsorptive removal of cationic and anionic dyes from aqueous solution by utilizing almond shell as bioadsorbent, Euro-Mediterranean Journal for Environmental Integration. 2

(2017) 20. doi:10.1007/s41207-017-0032-y.

[18] N. Maaloul, R. Ben Arfi, M. Rendueles, A. Ghorbal, M. Diaz, Dialysis-free extraction and characterization of cellulose crystals from almond (Prunus dulcis) shells, Journal of Materials and Environmental Science. 8 (2017) 4171–4181. doi:438-JMES-2556.

[19] A.A. Alshaheri, T.I. Mohamed, R.B. Abdul, B. Thahira, T.A. Saleh, Synthesis, characterisation and catalytic activity of dithiocarbazate Schiff base complexes in oxidation of cyclohexane, Journal of Molecular Liquids. 240 (2017) 486--496. doi:10.1016/j.molliq.2017.05.081.

[20] W.H. Danial, Z. Abdul Majid, M.N. Mohd Muhid, S. Triwahyono, M.B. Bakar, Z. Ramli, The reuse of wastepaper for the extraction of cellulose nanocrystals, Carbohydrate Polymers. 118 (2015) 165–169. doi:http://dx.doi.org/doi:10.1016/j.carbpol.2014.10.072.

[21] M.N. Belgacem, G.G. Silva, Characterization of three non-product materials from a bleached eucalyptus kraft pulp mill , in view of valorising them as a source of cellulose fibres, 7 (2007) 288–295. doi:10.1016/j.indcrop.2007.11.005.

[22] C. Popescu, P. Tomas, N. Olaru, C. Vasile, Spectroscopic study of acetylated kraft pulp fibers, Carbohydrate Polymers. 88 (2012) 530–536. doi:10.1016/j.carbpol.2011.12.046.

[23] V.A. Alvarez, A. Vazquez, Influence of fiber chemical modification procedure on the mechanical properties and water absorption of MaterBi-Y / sisal fiber composites, Composites: Part A. 37 (2006) 1672–1680. doi:10.1016/j.compositesa.2005.10.005.

[24] Priya, A.K. Sharma, B.S. Kaith, V. Tanwar, J.K. Bhatia, N. Sharma, S. Bajaj, S. Panchal, RSM-CCD optimized sodium alginate/gelatin based ZnS-nanocomposite hydrogel for the effective removal of biebrich scarlet and crystal violet dyes, International Journal of Biological Macromolecules. (2019). doi:10.1016/j.ijbiomac.2019.02.034.

[25] N. Rambabu, S. Panthapulakkal, M. Sain, A.K. Dalai, Production of nanocellulose fibers from pinecone biomass: Evaluation and optimization of chemical and mechanical treatment conditions on mechanical properties of nanocellulose films, Industrial Crops and Products. 83 (2016) 746–754. doi:http://dx.doi.org/10.1016/j.indcrop.2015.11.083.

[26] H. Zeghioud, N. Khellaf, A. Amrane, H. Djelal, W. Elfalleh, A.A. Assadi, S. Rtimi, Photocatalytic performance of TiO2 impregnated polyester for the degradation of Reactive Green 12: implications of the surface pretreatment and the microstructure, “Journal of Photochemistry and Photobiology, A: Chemistry.” 346 (2017) 493–501. doi:http://dx.doi.org/doi:10.1016/j.jphotochem.2017.07.005 JPC.

[27] L. Zhang, J. Tu, L. Lyu, C. Hu, Environmental Enhanced catalytic degradation of ciprofloxacin over Ce-doped OMS-2 microspheres, “Applied Catalysis B, Environmental.” 181 (2016) 561–569. doi:10.1016/j.apcatb.2015.08.029.

[28] C. Li, H. Lin, A. Armutlulu, R. Xie, Y. Zhang, Hydroxylamine-assisted catalytic degradation of ciprofloxacin in ferrate / persulfate system, Chemical Engineering Journal. (2018). doi:10.1016/j.cej.2018.11.218.

[29] A.A. Azzaz, A.A. Assadi, S. Jellali, A. Bouzaza, D. Wolbert, S. Rtimi, L. Bousselmi, Discoloration of simulated textile effluent in continuous photoreactor using immobilized titanium dioxide: Effect of zinc and sodium chloride, Journal of Photochemistry and Photobiology A: Chemistry. 358 (2018) 111–120. doi:https://doi.org/10.1016/j.jphotochem.2018.01.032.

[30] A.A. Azzaz, S. Jellali, A.A. Assadi, L. Bousselmi, Desalination and Water Treatment Chemical treatment of orange tree sawdust for a cationic dye enhancement removal from aqueous solutions : kinetic , equilibrium and thermodynamic studies, Desalination and Water Treatment. 57 (2016) 22107–22119. doi:10.1080/19443994.2015.1103313.

[31] J. Herrmann, H. Tahiri, C. Guillard, P. Pichat, Photocatalytic degradation of aqueous hydroxy-butandioic acid (malic acid) in contact with powdered and supported titania in water, 54 (1999) 131–141.

[32] J. Han, C. Zhou, A.D. French, G. Han, Q. Wu, Characterization of cellulose II nanoparticles regenerated from 1-butyl-3-methylimidazolium chloride, Carbohydrate Polymers. 94 (2013) 773–781. doi:http://dx.doi.org/10.1016/j.carbpol.2013.02.003.

[33] A.N. Módenes, F.R. Espinoza-Quiñones, C.A.Q. Geraldi, D.R. Manenti, D.E.G. Trigueros, A.P. De Oliveira, C.E. Borba, A.D. Kroumov, Assessment of the banana pseudostem as a low-cost biosorbent for the removal of reactive blue 5G dye, Environmental Technology. 36 (2015) 2892–2902. doi:10.1080/09593330.2015.1051591.

[34] M. fang Li, Y. guo Liu, S. bo Liu, D. Shu, G. ming Zeng, X. jiang Hu, X. fei Tan, L. hua Jiang, Z. li Yan, X. xi Cai, Cu(II)-influenced adsorption of ciprofloxacin from aqueous solutions by magnetic graphene oxide/nitrilotriacetic acid nanocomposite: Competition and enhancement mechanisms, Chemical Engineering Journal. 319 (2017) 219–228. doi:10.1016/j.cej.2017.03.016.

[35] W. Qian, Q. Song, H. Ding, W. Xie, Computational simulations of the mass transfer zone in GS adsorption column packed with Fe-type ion exchanger, Chemosphere. (2018). doi:10.1016/j.chemosphere.2018.10.054.

[36] M.K. Mondal, Removal of Pb (II) ions from aqueous solution using activated tea waste : Adsorption on a fixed-bed column, Journal of Environmental Management. 90 (2009) 3266–3271.

[37] M. Karimi, A. Shojaei, A. Nematollahzadeh, M.J. Abdekhodaie, Column study of Cr (VI) adsorption onto modified silica -polyacrylamide microspheres composite, Chemical Engineering Journal. 210 (2012) 280–288.

[38] S.K. Bajpai, M. Bajpai, N. Rai, Sorptive removal of ciprofoxacin hydrochloride from simulated wastewater using sawdust: Kinetic study and effect of pH, Water SA. 38 (2012) 673–682.

[39] T. Zadi, A.A. Assadi, N. Nasrallah, R. Bouallouche, P.N. Tri, A. Bouzaza, M.M. Azizi, R. Maachi, D. Wolbert, Treatment of hospital indoor air by a hybrid system of combined plasma with photocatalysis: case of trichloromethane, Chemical Engineering Journal. 349 (2018) 276–286.

[40] H. Zeghioud, A.A. Assadi, N. Khellaf, H. Djelal, A. Amrane, S. Rtimi, Reactive species monitoring and their contribution for removal of textile effluent with photocatalysis under UV and visible lights: dynamics and mechanism, “Journal of Photochemistry and Photobiology, A: Chemistry.” 365 (2018) 94–102.

[41] K.M. Reza, A. Kurny, F. Gulshan, Parameters affecting the photocatalytic degradation of dyes using TiO2: a review, Applied Water Science. 7 (2017) 1569–1578.

[42] J.H.O.S. Pereira, A.C. Reis, D. Queirós, O.C. Nunes, M.T. Borges, V.P. Vilar, R.A.R. Boaventura, Insights into solar TiO2-assisted photocatalytic oxidation of two antibiotics employed in aquatic animal production, oxolinic acid and oxytetracycline, Science of the Total Environment. 463–464 (2013) 274–283.

[43] D.D. Dionysiou, M.T. Suidan, E. Bekou, I. Baudin, J.M. Laîné, Effect of ionic strength and hydrogen peroxide on the photocatalytic degradation of 4-

chlorobenzoic acid in water, Applied Catalysis B: Environmental. 26 (2000) 153–171.

[44] H.K. Singh, M. Saquib, M.M. Haque, M. Muneer, Heterogeneous photocatalysed decolorization of two selected dye derivatives neutral red and toluidine blue in aqueous suspensions, Chemical Engineering Journal. 136 (2008) 77–81.

[45] C. Hu, J.C. Yu, Z. Hao, P.K. Wong, Effects of acidity and inorganic ions on the photocatalytic degradation of different azo dyes, Applied Catalysis B: Environmental. 46 (2003) 35–47.

[46] M.I. Maldonado, J. Blanco, W. Gernjak, S. Malato, P. Ferna, Decontamination and disinfection of water by solar photocatalysis : Recent overview and trends, 147 (2009) 1–59.

[47] A. Heller, The Role of Oxygen in Photooxidation of Organic Molecules on Semiconductor Particles, 0 (1991) 5261–5267.

[48] G. Chen, F. Liu, Y. Qiao, B. Tao, Photodegradation of tefuryltrione in water under UV irradiation: Identification of transformation products and elucidation of photodegradation pathway, Chemosphere. 227 (2019) 133–141.

Methodology of treatment

Water treated

Oxidation process: Photocatalysis

Adsorption

Regeneration